Nuclear Instruments and Methods in Physics Research A272 (1988) 564–573
North-Holland, Amsterdam

THREE DIMENSIONAL SIMULATION OF HIGH HARMONIC TRANSVERSE OPTICAL KLYSTRON *

S.K. DUTT, A. FRIEDMAN [1], A. GOVER [1] and C. PELLEGRINI

National Synchrotron Light Source, Brookhaven National Laboratory, Upton, New York 11973, USA
[1] Science Applications International Corporation, 1710 Goodridge Drive, McLean, VA 22102, USA

We present the results of a three dimensional simulation code, which calculates the parameters of coherent super-radiant harmonic frequency emission by electrons which are being bunched by an external laser beam while propagating in a planar undulator. This code was written in order to simulate the TOK experiment, which is presently underway at BNL. Instead of a full numerical simulation of Maxwell's equations and the electron force equations, a semi-analytical approach is adopted. Electron trajectories are computed analytically, and the radiation fields are expanded in terms of free space eigenmodes. Phase space and energy profiles of the electron beam are incorporated by a variable space sampling according to a given distribution function, rather than via Monte Carlo simulation. Computation time of about 0.1 s/electron was achieved with the present version of the code on the IBM 3090. We present the expected radiometric parameters as a function of the electron beam parameters (emittance and energy spread), and the modulating laser beam parameters (Rayleigh length, waist position and power). Statistical averaging is carried out by weighted averaging of the initial electron moments and energy phase space distribution. This approach results in the best prediction of the expected experimental measurement of the optical parameters which can be achieved with a finite number of sampling electrons (much smaller than in the experiment), without introducing artificial noise as in the Monte Carlo approach.

1. Introduction

FEL3D is a three dimensional simulation code for the transverse optical klystron (TOK) experiment presently underway at the National Synchrotron Light Source. The program is capable of simulating the coherent super-radiant harmonic frequency emission from electrons interacting with an external laser beam while propagating in an undulator. The code is based on a semi-analytic concept: instead of a full numerical solution of the coupled Maxwell–Lorentz equations, electron trajectories within the undulator are approximated by analytic solutions, and the radiation fields are expanded in terms of free space eigenmodes (Hermite–Gauss modes, or plane waves). This approach is well justified in the optical regime [1,2], and has the advantage of shortening computation time. ** FEL3D incorporates the important three dimensional features of

– the electron beam: spread in the transverse coordinates and velocities, as well as in the beam energy, can be specified according to a given probability distribution function;
– the modulating laser beam: this is achieved by using a fundamental Hermite–Gauss mode with independent transverse focusing parameters.

In section 2 of this paper, we present a summary of the physical model on which FEL3D is based. In section 3, we discuss the statistical averaging method used to determine the phase space and energy profiles of the electron beam as it enters the undulator. It is important to note that we do not use Monte Carlo methods in determining these distributions, thereby avoiding the introduction of unphysical noise in the simulation. Section 4 deals with the user-interactive features of FEL3D, and details the capabilities of the program. Section 5 concerns itself with a number of tests which probe the accuracy of the simulation code, and, by implication, the physical model itself. Finally, we provide sample output from FEL3D in section 6, and discuss the significance of our results for the Brookhaven TOK experiment.

* Research carried out under the auspices of the U.S. Department of Energy. Work supported in part by ONR contract No. N00014-87-C-0362.

** Scalar implementations of FEL3D on the BNL IBM 3090 yield an average CPU time of $\lesssim 0.1$ seconds per electron. The vectorized code is expected to run significantly faster.

0168-9002/88/$03.50

2. The physical model

In this section we summarize the theoretical model underlying FEL3D. A more detailed description description of the relevant theory can be found in earlier publications [3,4].

2.1. Spontaneous and super-radiant undulator emission

The TOK consists essentially of a periodic magnetic structure – the undulator, or wiggler, magnet – which

Table 1
Definitions of the various harmonics involved in undulator synchroton radiation and super-radiant emission.

Frequency	definition	linewidth
fundamental undulator frequency	$\omega_u = \frac{k_u c}{\beta_z^{-1} - 1} \approx 2\gamma_z^2 k_u c$	$\frac{\Delta\omega_u}{\omega_u} = \frac{1}{N_u}$
modulating laser frequency	$\omega_m \approx m\omega_u$	$\frac{\Delta\omega_m}{\omega_m} = \frac{2\pi/T_{laser}}{\omega_m}$
nth order coherent laser harmonic	$\omega_n = n\omega_m \approx nm\omega_u$	$\frac{\Delta\omega_n}{\omega_n} = \frac{2\pi/T_{pulse}}{\omega_m}$
lth order incoherent undulator harmonic	$\omega_{ul} = l\omega_u$	$\frac{\Delta\omega_{ul}}{\omega_{ul}} = \frac{1}{lN_u}$

induces transverse quiver motion in the trajectory of electrons propagating along it. The transverse quiver motion of a single electron produces coherent Doppler-shifted radiation. This radiation is emitted predominantly in the forward direction at a central frequency

$$\omega_u = \frac{k_u c}{\beta_z^{-1} - 1} \approx 2\gamma_z^2 k_u c,$$

and at all odd harmonics $\omega_{ul} = l\omega_u$ of the central frequency *. While the undulator synchroton radiation from any single electron is temporally and spatially coherent, individual electrons within the undulator emit at random phase relative to each other because they enter the undulator at random times. Consequently, the undulator synchroton radiation is only partially coherent. This radiation can be made coherent by bunching the electrons along the undulator axial dimension with the aid of an external laser beam oscillating at one of the undulator harmonics, and propagating collinearly with the electron beam. If the density modulation is tight enough, it contains harmonics of the laser frequency, and the bunched electrons emit super-radiant coherent radiation at the laser frequency ω_m and its odd

* Note that $k_u = 2\pi/\lambda_u$ is the undulator wave number, $\beta_z = v_z/c$, and $\gamma_z \equiv (1-\beta_z^2)^{1/2}$; l is an odd integer.

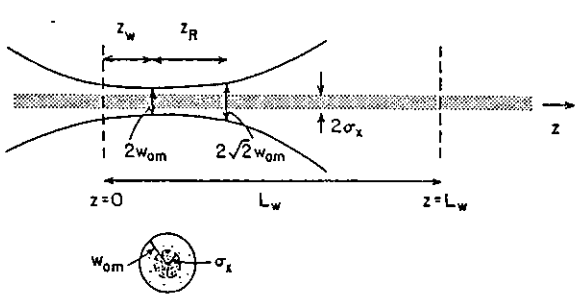

Fig. 1. Axial and transverse cross-sectional schematics of the electron beam and the modulating laser beam for the Brookhaven TOK experiment.

Table 2
Summary of emission schemes

1 Undulator Synchrotron Radiation FEL Spontaneous Emission):
The temporally incoherent radiation of electrons propagating in an undulator.

2 Super-Radiant Free Electron Radiation:
The temporally coherent radiation of bunched electrons oscillating in phase with each other in an undulator.

3 Free Electron Lasing:
The coherent emission of bunched electrons radiating in phase into the same spatial and frequency domain as the radiation field which produced the bunching.

harmonics $n\omega_m$. Fig. 1 illustrates the experimental setup of the Brookhaven TOK experiment. The external laser beam is focused at the undulator entrance, and density modulation of the electron beam is achieved towards the end of the undulator. Table 1 summarizes the definitions of the various harmonics involved in undulator synchroton radiation and super-radiant emission.

The TOK represents a scheme for greatly enhancing the spectral brightness of undulator harmonic radiation. While the total power radiated is not different, it can be made substantially more coherent without involving any stimulated radiation as in the case of a free electron laser (FEL). Further, in contrast to the FEL, there is no oscillation threshold condition to be satisfied in order to obtain coherent harmonic emission. Consequently, the optical klystron is of particular interest in the short wavelength (VUV) range, where the FEL oscillation condition is hard to satisfy. The different emission schemes which apply to the electron beam are summarized in table 2.

2.2. Electron trajectories and equations of motion

For practical experimental parameters in the optical regime, the detailed solution of the coupled system of

Maxwell–Lorentz equations can be substantially simplified by three assumptions:
- Space charge effects may be ignored since the electron beam operates in the extreme-relativistic regime.
- Electron trajectories are not affected by the emitted radiation fields since the electron beam loses only a small fraction of its energy via undulator super-radiant emission.
- Electron *transverse* trajectories are determined solely by the undulator field. The transverse field of the modulating laser beam produces high-frequency, small-amplitude quiver in electron transverse motion, which may be ignored in comparison to the slower *longitudinal* quiver arising from the beating of the laser field with the undulator field.

These assumptions effectively decouple the electron radiation and modulation problems. If, in addition, one averages over the longitudinal quiver motion, an approximate set of equations describing the energy and phase of the electrons is obtained. By expressing the force equations in terms of the relativistic proper time $\tau_j \equiv \int_{t_{j0}}^{t} \mathrm{d}t'/\gamma_j(t')$ for the jth electron, the equations can be reduced into a pendulum-like equation for the electron phases [1,2]:

$$\frac{\mathrm{d}\gamma_j}{\mathrm{d}\tau_j} = \tfrac{1}{2}(-1)^{(n-1)/2}\frac{eE(x_j, y_j, z_j, t)}{m_e c} \times K\left[J_{(n-1)/2}(u) - J_{(n+1)/2}(u)\right] \times \sin\left[\psi_{mj} + \Phi_m(x_j, y_j, z_j)\right],$$

$$\frac{\mathrm{d}\psi_{mj}}{\mathrm{d}\tau_j} = \frac{k_m + mk_u}{m_e} p_{jz} - \omega_m \gamma_j.$$

$K \equiv eBu/m_e c^2 k_u$ is the undulator parameter, $\psi_{mj} \equiv (k_m + mk_u)z_j(t) - \omega_m t$, and

$$u \equiv \frac{\omega_m}{8k_u}\frac{K^2}{c\beta_z \gamma^2} \approx \frac{m}{4}\frac{K^2}{1 + K^2/2}.$$

The modulating laser beam field is taken to be the fundamental Hermite–Gauss mode, with independent traverse focusing parameters z_{R_x} and z_{R_y}, and beam waist sizes $w_x(0)$, $w_y(0)$:

$$E(x, y, z, t) = e_x E_0 \frac{w_x(0)w_y(0)}{w_x(z)w_y(z)} \times \mathrm{Re}\left[\exp\left(-\frac{x^2}{w_x^2(z)} - \frac{y^2}{w_y^2(z)} + \mathrm{i}\Phi_m(x, y, z) + \mathrm{i}\frac{\omega_m}{c}z - \mathrm{i}\omega_m t\right)\right].$$

Note that

$$\Phi_m(x, y, z) = \frac{\omega_m}{4c}\left(\frac{x^2}{R_x(z)} + \frac{y^2}{R_y(z)}\right) - \frac{1}{2}\left[\tan^{-1}\left(\frac{z - z_{w_x}}{z_{R_x}}\right) + \tan^{-1}\left(\frac{z - z_{w_y}}{z_{R_y}}\right)\right],$$

$$R_{x,y} = (z - z_{w_{x,y}})\left[1 + \frac{z_{R_{x,y}}^2}{(z - z_{w_{x,y}})^2}\right],$$

$$z_{R_{x,y}} = \pi w_{x,y}^2(0)/\lambda_m.$$

This 3-D model field affects even electrons *on axis*, since they experience an electromagnetic wave with varying amplitude and phase along the interaction length. The longitudinal quiver has been averaged away, leaving the various Bessel function factors, and producing the average constant of the motion [5]:

$$\left[J_{(n-1)/2}(u) - J_{(n+1)/2}(u)\right]\omega_m p_{jz} - \left[(k_m + k_u)J_{(n-1)/2}(u) - (k_m - k_u)J_{(n+1)/2}(u)\right] m_e c^2 \gamma_j = \text{constant}_j.$$

The schematic laser beam and electron beam focussing parameters are illustrated in fig. 1. The laser beam, at the frequency of a doubled Nd–YAG laser, is illuminating the electron beam at the third ($m = 3$) harmonic of the fundamental undulator frequency ω_u.

3. The statistical averaging method

The principal features of the statistical averaging procedure in FEL3D are detailed below:

(1) We assume that electrons are injected into the undulator with a uniform distribution in the time domain. For a given choice N_ϕ of electrons representing the initial phase distribution in an optical period, a one-period phase region $-\pi/2 \le \psi_{j0} \le 3\pi/2$ is divided into N_ϕ equal segments, and one electron is placed in the center of each segment. This procedure ensures that unintended pre-bunching effects do not show up in the simulation results. The number of electrons N_ϕ is chosen according to the highest harmonic frequency for which bunching and radiation data are to be computed. The Nyquist theorem suggests that the minimum number of sampling electrons required for simulating laser harmonics up to and including $n_{\max}$ is given by

$$N_\phi = 4n_{\max}.$$

This number should also be sufficient, as is indeed the case for output from FEL3D, which remains unchanged

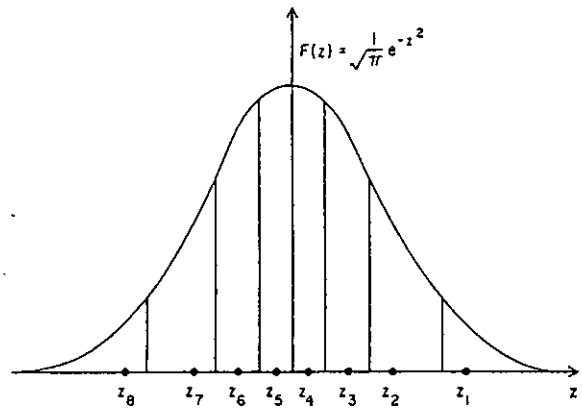

Fig. 2. Sampling algorithm: The distribution is split into $N = 8$ equals area sections and the sampling electrons are located in the center of gravity of each section.

if the number of phases is increased beyond the Nyquist criterion.

(2) Arbitrary distribution functions can be used for sampling the electron initial conditions in the transverse coordinates x_j, y_j, angles ϕ_{xj}, ϕ_{yj}, and energy γ_j. The present program is written with the assumption of a Gaussian distribution in all five variables, which is a good approximation for storage ring beams. For proper sampling of the Gaussian distribution function the normalized Gaussian $F(z) = e^{-z^2}/\sqrt{\pi}$ is divided into N equal-area segments as shown in fig. 2, where N is the number of electrons being sampled in a given dimension of the 5-D space $(x, y, \phi_x, \phi_y, \gamma)$. One sample electron is then placed in the center of gravity of each of the N equal-area segments. There is no simple estimate of the number of electrons required for representative sampling in each phase space dimension. A choice of 8 electrons per dimension gave consistent results for computation of on-axis radiative emission, although more sampling points may be required for a reliable estimate of off-axis radiation parameters.

(3) Since the undulator structure, the modulating laser beam, and the distribution functions all satisfy symmetry of reflection $x \to -x$ and $y \to -y$, the dynamics of an electron with initial conditions (x_0, ϕ_{x0}) is identical to that of an electron at $(-x_0, -\phi_{x0})$. Consequently, the simulation code can take advantage of this symmetry by sampling only half of the phase space distribution in the (x, ϕ_x) and (y, ϕ_y) planes, resulting in a two-fold reduction in computation time. The symmetric sampling procedure is illustrated in fig. 3.

(4) The five-dimensional electron distribution function factorizes at any transverse plane within the undulator according to

$$f(x, \phi_x, y, \phi_y, \gamma) = f_x(x, \phi_x)\, f_y(y, \phi_y)\, f_\gamma(\gamma).$$

The distribution functions f_x, f_y of each of the conjugate phase space variables (x, ϕ_x), (y, ϕ_y) factorize at waist positions z_{E_x}, z_{E_y}. These may be different if the focusing parameters of the electron beam are different in the two transverse dimensions, as is usually the case with storage ring beams. The sampling procedure described above is carried out for each phase space dimension at its corresponding waist position, and the initial conditions at the undulator entrance ($z = 0$) are computed by the traceback transformation

$$x_j(0) = x_{j0} - z_{E_x}\phi_{xj0},$$

$$\phi_{xj}(0) = \phi_{xj0}.$$

(x_{j0}, ϕ_{xj0}) are the coordinates at the waist, and $(x_j(0), \phi_{xj}(0))$ are the coordinates at $z = 0$. Corresponding expressions for the y-dimension may be obtained with the substitution $x \to y$.

The distribution function averaging adopted here is more appropriate than the Monte Carlo approach which is sometimes taken in simulation programs. In the Monte Carlo approach one distributes electron initial conditions via a random number generator weighed by the known statistical distribution function. This introduces an amount of noise in the computed values of the physical parameters. Since the noise in the measured parameters is determined by fluctuations in the actual electron beam (shot noise) due to the large number of electrons in the beam, and since these fluctuations are expected to be smaller than those induced by the Monte Carlo method, we expect our approach to produce a closer match between simulated and measured values of the radiative emission parameters. We note finally that if, in the experiment, the measured parameter values fluctuate because of fluctuations in the electron beam, the simulated parameter values should correspond to the measured parameters averaged over many experiments.

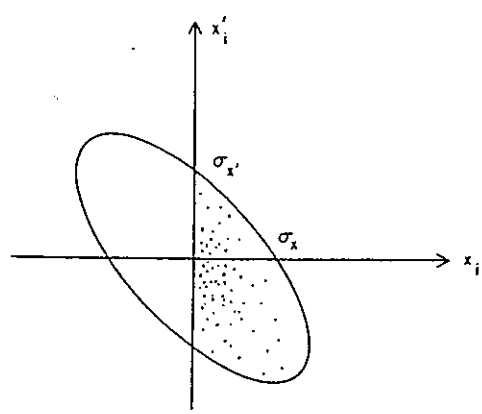

Fig. 3. The meaning of symmetry in initial conditions: when symmetry $(x \to -x, x' \to -x')$ is taken advantage of, only the shaded part of the distribution is sampled, representing the entire distribution.

IV. SIMULATION

4. FEL3D program features

FEL3D is designed to interact with the user at his terminal. The code consists of two separate programs called PINPUT and PENTOK. In this section we detail the user-interactive features of the code, and describe the parameters which it computes.

4.1. Program PINPUT

Program PINPUT contains all the user-interactive features of FEL3D. Its purpose is to prepare a data file containing
- the physical parameters which characterize the undulator, the modulating laser beam, and the electron beam;
- the phase space and energy profiles of the electron beam at the undulator entrance, using the method described in section 3.

PINPUT contains an internal data base with representative values for all user-changeable parameters. This data base is invoked the first time FEL3D is run. Subsequent runs do not invoke the internal data if the user instructs PINPUT at the end of a terminal session to prepare a file containing the values generated by the user. This file can be updated every time FEL3D is run, and serves as the primary file read by PINPUT. The first set of parameters displayed by PINPUT is shown in table 3.

The user may change any or all of the above parameters by first entering the number next to a particular parameter. PINPUT provides the current value of that parameter, and prompts the user for the new value. This process of changing the characteristics of the undulator and the modulating laser beam may be terminated after any number of entries. Alternatively, the user may elect to change all the parameters one by one. The code will then lead the user through the entire table shown above.

Table 3
FEL parameter group

(1) λ_w (m) 0.1	(2) N_w 22	(3) $\bar{a}_w$ 4.31
(4) λ_L (m) 0.532×10^{-6}	(5) Z_R (m) 0.5	(6) Z_w (m) 0.3
(7) P_L (W) 0.6×10^{8}	(8) γ 783.14	(9) n_{max} 9
(10) ΔZ (m) 0.05	(11) N_{steps} 440	(12) ϵ 0.1×10^{-6}

A brief description of each parameter follows:
(1) The undulator period (meters).
(2) Number of undulator periods.
(3) R.M.S. undulator parameter.
(4) Modulating laser wavelength (meters).
(5) Modulating laser Rayleigh length (meters).
(6) Modulating laser waist position (meters).
(7) Modulating laser power (watts).
(8) Electron beam energy. If the beam is not monochromatic, this is the central value of a Gaussian distribution.
(9) Highest harmonic of the output radiation field for which bunching and super-radiant harmonic emission data are to be computed.
(10) Integration step size (meters).
(11) Total number of integration steps taken along the undulator length. Note that parameters 10 and 11 are not independent. Specifying any one leads to the other being calculated internally.

Table 4
Electron beam parameter group

(1) X Y	(2) X' Y	(3) Y N	(4) Y' N	(5) γ Y		
(6) N_x 10	(7) $N_{x'}$ 10	(8) N_y 1	(9) $N_{y'}$ 1	(10) N_γ 10	(11) N_ϕ 20	(12) m 3
(13) Symm X Y	(14) Symm Y Y					
(15) σ_x 0.9126E−02	(16) $\sigma_{x'}$ 0.1157E−03	(17) σ_y 0.1368E−02	(18) $\sigma_{y'}$ 0.1083E−03	(19) σ_γ 0.1768E−03		
(20) X_b 0.2724E−02	(21) X'_b 0.1636E−03	(22) Y_b 0.1960E−02	(23) Y'_b 0.1531E−03	(24) γ_b 0.2500E−03		
(25) β_x 0.1120E+02	(26) ϵ_x 0.1500E−06	(27) ϵ_x^* 0.9425E−06	(28) β_y 0.1280E+02	(29) ϵ_y 0.1500E−06	(30) ϵ_y^* 0.9425E−06	

(12) Accuracy desired of the computation. This parameter is defined by the numerical integration routine which is used to calculate electron trajectories [6,7].

PINPUT next displays a second table of parameters, see table 4, which allow one to specify the characteristics of the electron beam. A brief description of the above parameters follows:

(1–5) Spread in the transverse coordinates and velocities, and in the beam energy are indicated by entering Y or N.

(6–10) The number of Gaussian distributed transverse coordinates, velocities, and energies.

(11) Number of electrons per wavelength. As mentioned in section 3, by the Nyquist criterion one should choose $N_\phi = 4n_{max}$ at the minimum. This should also be sufficient.

(12) Harmonic of the fundamental undulator frequency at which the modulating laser beam is operating. For the TOK experiment at BNL, this value is 3.

(13,14) Indicates whether the phase space distribution is taken to be symmetric, as shown in fig. 3. Choosing symmetry leads to a two-fold reduction in computation time.

(15–19) Standard deviation values for spread in a given dimension.

(20–30) The parameters in this subgroup allow one to use alternative methods of characterizing the Gaussian spread. The following definitions are of relevance:

$$X_b \equiv \sqrt{2}\,\sigma_x, \qquad X_b' \equiv \sqrt{2}\,\sigma_{x'},$$

$$Y_b \equiv \sqrt{2}\,\sigma_y, \qquad Y_b' \equiv \sqrt{2}\,\sigma_{y'},$$

$$\gamma_b \equiv \sqrt{2}\,\sigma_\gamma,$$

$$\beta_x \equiv \sigma_x^2/\epsilon_x, \qquad \epsilon_x \equiv \sigma_x\sigma_{x'}, \qquad \epsilon_x^* \equiv 2\pi\epsilon_x,$$

$$\beta_y \equiv \sigma_y^2/\epsilon_y, \qquad \epsilon_y \equiv \sigma_y\sigma_{y'}, \qquad \epsilon_y^* \equiv 2\pi\epsilon_y.$$

For any independent choice of spread parameters, such as σ_x and $\sigma_{x'}$, PINPUT computes and displays the corresponding values of the other possible choices. The user may change the parameters in the electron beam group according to the scheme described earlier for the first parameter group.

4.2. Program PENTOK

This is the second program in the simulation code for the BNL TOK. PENTOK does not require any user interaction. It reads the data file prepared by PINPUT and invokes a numerical integration routine [6,7] to compute electron phase space trajectories. The trajectory data is used to compute the harmonic frequency bunching $|\eta_n|$, radiated power P_n, and brightness B_n as defined below:

$$\eta_n \equiv \langle e^{-in\psi_{mj}} \rangle_j, \quad \text{where } \langle(\,)\rangle_j \equiv \frac{1}{N}\sum_{j=1}^{N}(\,)_j,$$

$$r_n(z) \equiv \frac{1}{\lambda_u}\int_0^z \eta_n(z')\,dz',$$

$$P_n(z) \equiv \frac{1}{I_0^2}\left(\frac{dP_{SR}^n}{d\Omega}\right)_{\theta=0}$$

$$= \frac{1}{16}\sqrt{\frac{\mu_0}{\epsilon_0}}\left(n\frac{\lambda_u}{\lambda_m}\right)^2\left(\frac{\bar{K}}{\gamma}\right)^2 [JJ]_l^2\,|r_n(z)|^2,$$

$$B_n(z) \equiv \frac{1}{I_0}\frac{(dP_{SR}^n/d\Omega)_{\theta=0}}{(dP_{UR}^n/d\Omega)_{\theta=0}} = \frac{1}{4}\frac{I\lambda_u^2}{ec}\frac{|r_n(z)|^2}{z}.$$

Note that $[JJ]_l \equiv J_{(l-1)/2}(lu) - J_{(l+1)/2}(lu)$, where $l = mn$ with $m = 3$. The index n characterizes the harmonic of the laser fundamental frequency ω_m. I_0 is the electron beam peak current. For the BNL TOK experiment, I_0 is expected to be about 30 A.

5. FEL3D code tests

The simulation code has been tested by examining the scaling laws for bunching and super-radiant harmonic power emission as a function of undulator length. For the case of a low power laser beam ($P_L \approx 10$ MW) with a Rayleigh length comparable to the length of the undulator, and for a monochromatic electron beam with no transverse spread, one expects the results of a one-dimensional analysis to be valid. The scaling

Table 5
Least square fit of scaling laws. Theoretical values for bunching and radiation: $|\eta_1| \propto z^2$, $P_1 \propto z^6$; $|\eta_3| \propto z^6$, $P_3 \propto z^{14}$; $|\eta_5| \propto z^{10}$, $P_5 \propto z^{22}$.
$P_L = 10$ MW, $z_R = 2$ m, $z_w = 0.5$ m.
No transverse or energy spread.

Harmonic number	Wiggler length (meters)	L.S.F. value of exponent	
		η_n	P_n
1	0.0–0.6	2.24	6.63
	0.0–2.2	2.10	6.29
	1.0–2.2	1.92	5.96
3	0.0–0.6	3.34	7.30
	0.0–2.2	5.05	11.46
	1.0–2.2	5.78	13.75
5	0.0–0.6	0.15	2.48
	0.0–2.2	4.56	9.37
	1.0–2.2	9.64	21.46

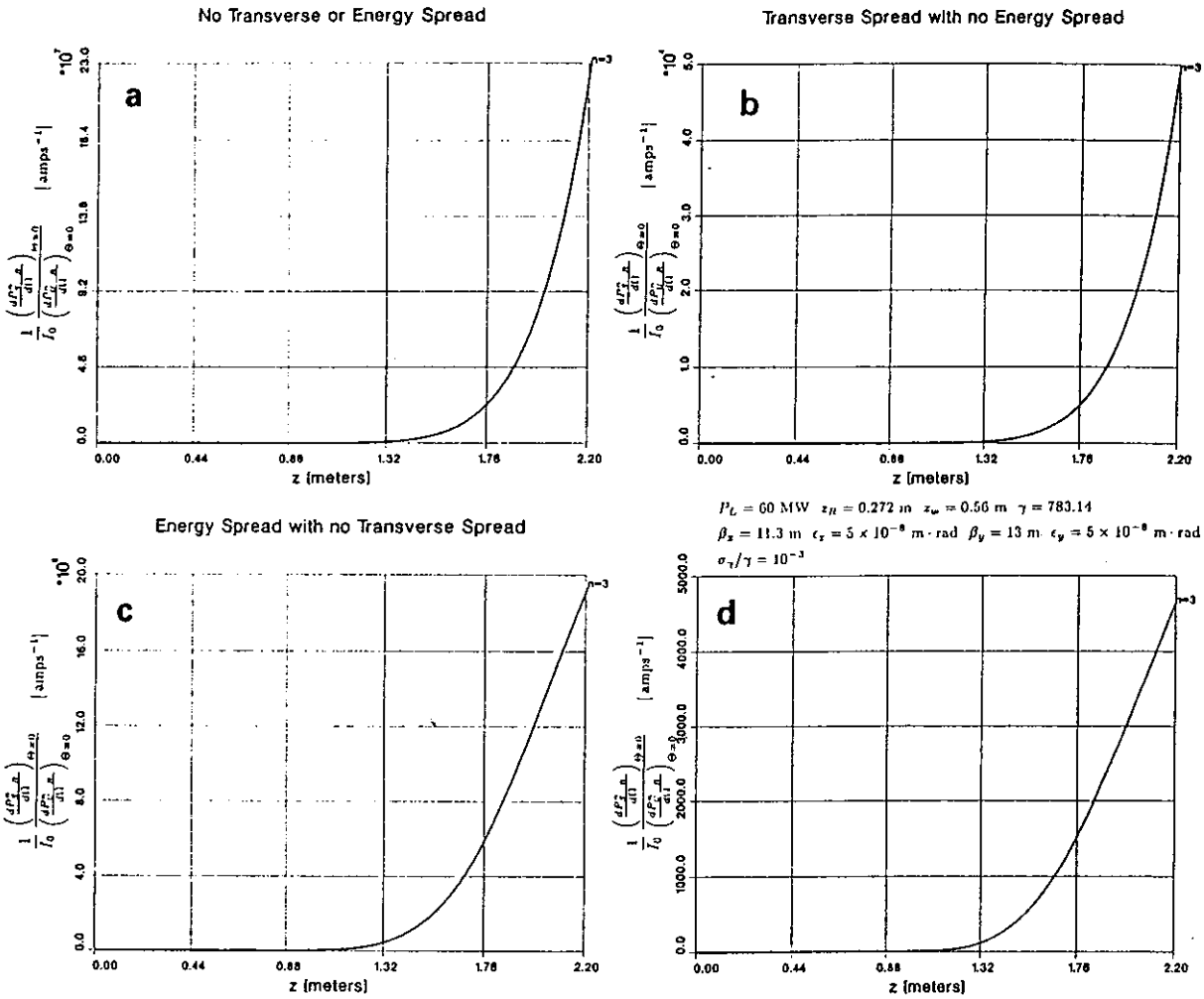

Fig. 4. Simulation results for the third harmonic. The figure displays the relative effect of transverse spread (b), energy spread (c), and their combined effect (d) on the ideal beam (a).

laws for the one-dimensional case can be calculated analytically, leading to the following results:

$$|\eta_n| \propto z^{2n},$$

$$P_n \propto z^{4n+2}, \quad n = 1,3,\cdots.$$

In table 5 we display the results from a least square fit analysis of the data obtained by fitting $\log|\eta_n|$, and $\log P_n$, versus $\log z$.

Note that the simulation data in the first half of the undulator is at or below the noise level for the computational process. This is indicated by the fact that the values of the scaling exponents calculated from the least square fit analysis match the one-dimensional predictions for the higher order harmonics only poorly. In the second half of the undulator, however, the scaling exponents are very close to the predicted values even for the higher order harmonics. We mention that while the data for bunching does not depend significantly on the step size chosen within the undulator, the radiation data does. This is because the radiation is computed from the bunching by simple Trapezoidal integration. If one chooses a very small step size within the undulator, however, one finds that the brightness factor increases by as much as 20% for the higher order harmonics. This increase in accuracy is paid for by a proportionate increase in computation time.

6. Simulation results and discussion

Simulation results for the third, fifth and seventh harmonics are displayed in figs. 4, 5, and 6 respectively. Each figure is subdivided into four parts to show the relative effects of energy spread and transverse spread

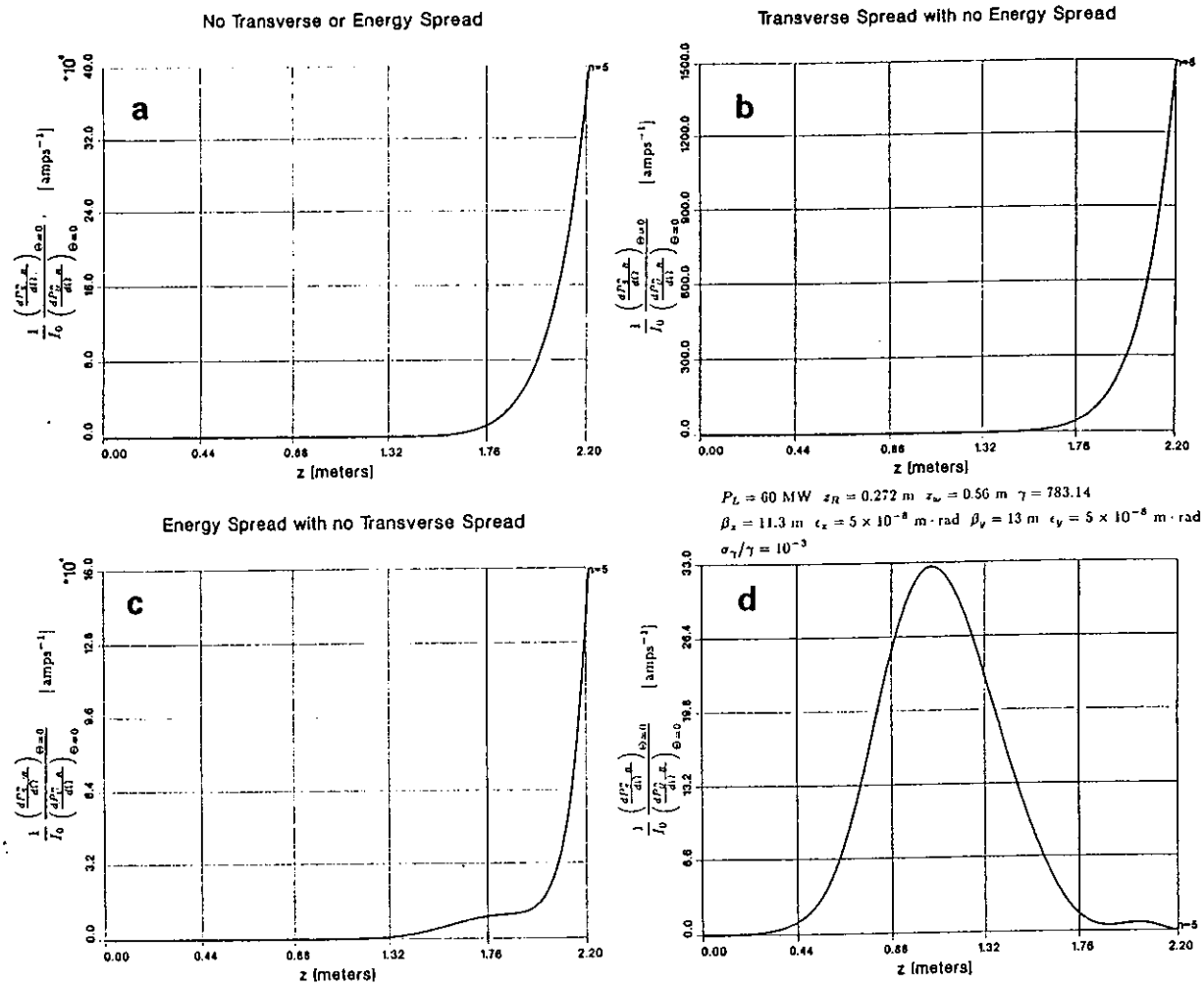

Fig. 5. Simulation results for the fifth harmonic. The figure displays the relative effect of transverse spread (b), energy spread (c), and their combined effect (d) on the ideal beam (a).

upon the brightness ratio, as well as the combined effect of the two *.

As is evident from the figures displayed, the effect of transverse spread dominates over the effect of energy spread, but in a markedly differently manner. Note that while the effect of transverse spread reduces the ideal brightness ratios in figs. 4a, 5a, and 6a by a factor ranging between 10^2 and 10^5, it leaves the qualitative nature of the growth in brightness unchanged. The effect of energy spread, on the other hand, is qualitatively very significant. The bunching peaks near the end of the undulator for the third harmonic, as is seen in fig. 7a. For the fifth harmonic the bunching reaches a relative maximum near the end of the undulator, reduces sharply and then builds up rapidly in the remaining length, as is shown in fig. 7b. The seventh harmonic, on the other hand, grows smoothly within the undulator. The corresponding brightness ratios in figs. 4c, 5c, and 6c are smoother as they are obtained by integrating the bunching factor along the undulator length. Note that quantitatively the effect of energy spread is considerably less significant than transverse spread, leading to a reduction in the brightness not exceeding a factor of 10^2.

When both transverse and energy spread are taken into account, the fifth harmonic is seen in fig. 5d to peak around the middle of the undulator, and to becoming insignificant at its end. The seventh harmonic, on the other hand, should be observable for the experimen-

* It is pertinent to mention that the undulator spontaneous radiation $(\mathrm{d}P''_{UR}/\mathrm{d}\Omega)_{\theta=0}$ used in computing the brightness ratio is calculated without taking into account the effect of spread in energy and in transverse positions and velocities. Accordingly, the brightness ratio should increase when these effects are accounted for.

IV. SIMULATION

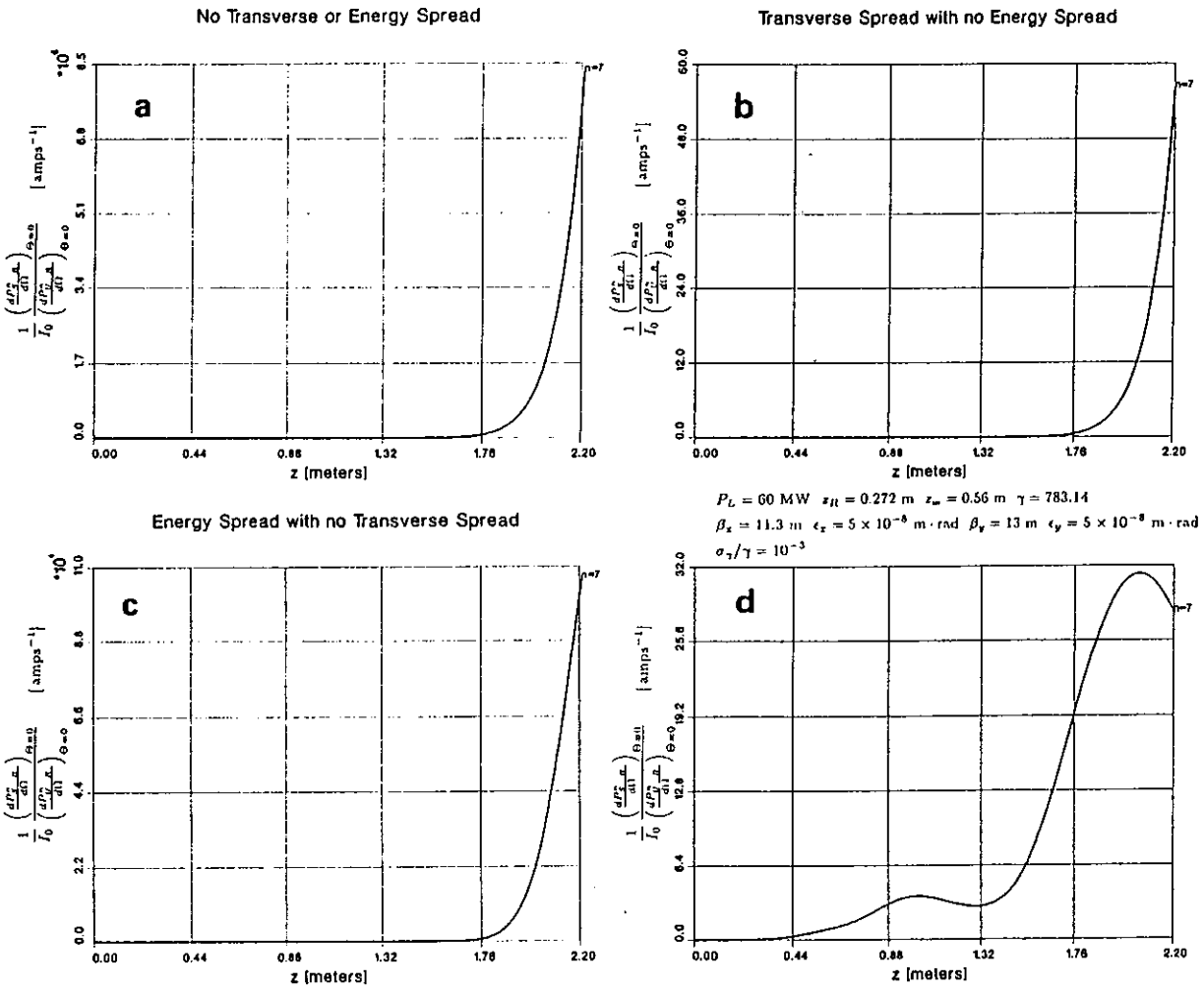

Fig. 6. Simulation results for the seventh harmonic. The figure displays the relative effect of transverse spread (b), energy spread (c) and their combined effect (d) on the ideal beam (a).

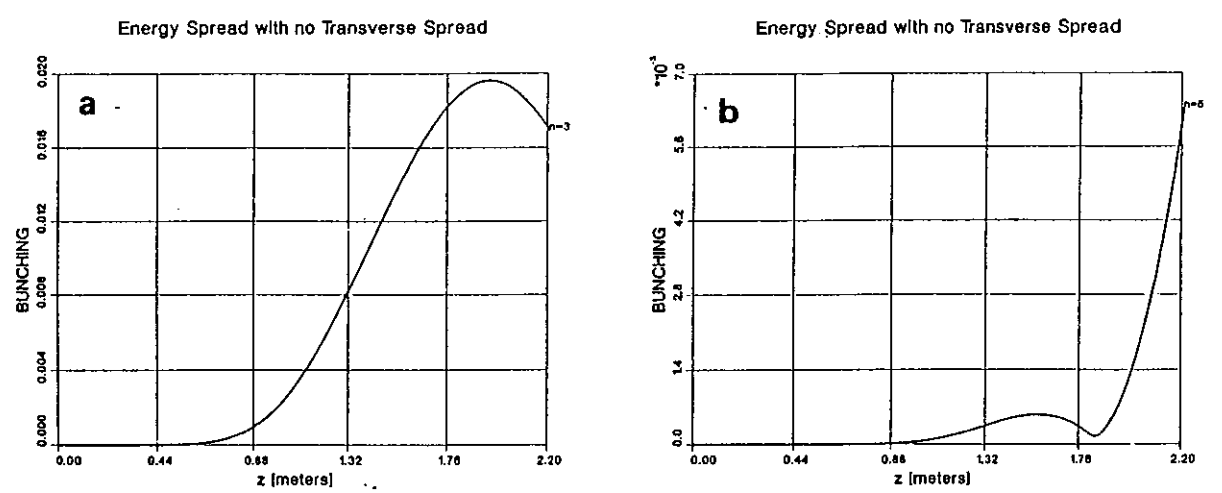

Fig. 7. Effect of energy spread on the bunching profile for the third harmonic (a) and the fifth harmonic (b).

tal conditions obtaining for the Brookhaven TOK experiment. This offers the prospect of validating our physical model from the experimental results.

References

[1] A. Gover, A. Friedman and A. Lucio, Proc. 8th Int. FEL Conf. Glasgow, UK (1986) ed. M.W. Poole, Nucl. Instr. and Meth. A259 (1987) 163.
[2] A. Gover, A. Luccio, A. Friedman and A.M. Fauchet, AIP Conf. Proc. 147 (1986) 219.
[3] G. Vignola, R.R. Freeman, B.M. Kincaid, C. Pellegrini, A. Lucio, J. Murphy, J. Galayda and A. van Steenbergen, Nucl. Instr. and Meth. A239 (1985) 43.
[4] B. Girard, Y. Lapierre, J.M. Ortega, C. Bazin, M. Billardon, P. Elleaume, M. Bergher, M. Velghe and Y. Petroff, Phys. Lett. 53 (1984) 2405.
[5] N.S. Ginsburg and M.D. Tokman, Sov. Phys. – Tech. Phys. 29 (6) (1984) 604.
[6] C.W. Gear, Numerical Initial Value Problems in Ordinary Differential Equations (Prentice-Hall, Englewoods Cliffs, NJ, 1971).
[7] W.H. Press, B.P. Flannery, S.A. Teukolsky and W.T. Vetterling, Numerical Recipes (Cambridge Univ. Press, Melbourne, 1986).